Title

Linear viscoelasticity of human sclera and posterior ocular tissues during tensile creep.

Authors

Song, Dooseop
Lim, Seongjin
Park, Joseph
et al.

Publication Date

2023-04-01

DOI

10.1016/j.jbiomech.2023.111530

Peer reviewed

HHS Public Access

Author manuscript

J Biomech. Author manuscript; available in PMC 2024 September 17.

Published in final edited form as:

J Biomech. 2023 April ; 151: 111530. doi:10.1016/j.jbiomech.2023.111530.

Linear Viscoelasticity of Human Sclera and Posterior Ocular Tissues During Tensile Creep

Dooseop Song[1,2], **Seongjin Lim**[1,2], **Joseph Park**[2], **Joseph L. Demer**[2,3,4]

[1]Department of Mechanical Engineering, University of California, Los Angeles.

[2]Department of Ophthalmology, Stein Eye Institute, University of California, Los Angeles.

[3]Department of Bioengineering, University of California, Los Angeles.

[4]Department of Neurology, University of California, Los Angeles.

Abstract

Purpose: Despite presumed relevance to ocular diseases, the viscoelastic properties of the posterior human eye have not been evaluated in detail. We performed creep testing to characterize the viscoelastic properties of ocular regions, including the sclera, optic nerve (ON) and ON sheath.

Methods: We tested 10 pairs of postmortem human eyes of average age 77 ± 17 years, consisting of 5 males and 5 females. Except for the ON that was tested in native shape, tissues were trimmed into rectangles. With physiologic temperature and constant wetting, tissues were rapidly loaded to tensile stress that was maintained by servo feedback as length was monitored for 1,500 sec. Relaxation modulus was computed using Prony series, and Deborah numbers estimated for times scales of physiological eye movements.

Results: Correlation between creep rate and applied stress level was negligible for all tissues, permitting description as linear viscoelastic materials characterized by lumped parameter compliance equations for limiting behaviors. The ON was the most compliant, and anterior sclera least compliant, with similar intermediate values for posterior sclera and ON sheath. Sensitivity analysis demonstrated that linear behavior eventually become dominant after long time. For the range of typical pursuit tracking, all tissues exhibit Debora numbers less than 75, and should be regarded as viscoelastic. With a 6.7 Deborah number, this is especially so for the ON during pursuit and convergence.

Conclusions: Posterior ocular tissues exhibit creep consistent with linear viscoelasticity necessary for describing biomechanical behavior of the ON, its sheath, and sclera during physiological eye movements and eccentric ocular fixations.

Address for Correspondence and Reprints: Joseph L. Demer, M.D., Ph.D. Stein Eye Institute, 100 Stein Plaza, UCLA, Los Angeles, California, 90095-7002 U.S.A. Facsimile: 310-206-7826, jld@jsei.ucla.edu.

Meeting Presentation: None.

Conflict of Interest:
No conflicting relationship exists for any author.

CRediT Statement

Dooseop Song: Investigation, Data curation, Software, Writing – original draft preparation. **Seongjin Lim:** Investigation, Methodology, Software, Validation, Writing – Reviewing and Editng. **Joseph Park**: Investigation, Methodology, Writing- Reviewing and Editing. **Joseph L. Demer**: Conceptualization, Supervision, Writing- Reviewing and Editing.

Keywords

creep; viscoelasticity; optic nerve; optic nerve sheath; sclera

1. Introduction

Although most ocular functions are tested clinically when at seemingly at rest, the eye is a highly dynamic organ that must undergo one to two micro-saccades per second, interspersed with drifts and other fixational eye movements, in order to avoid perceptual fading and optimize vision (Ghasia and Wang, 2022). The eye's nearly incessant motion (Kowler, 2011) represents a source of stresses and strains on ocular tissues, so it is important to understand the viscoelastic properties of the human eye and orbital tissues (Boote et al., 2020). One such viscoelastic characterization is creep, time-dependent inelastic deformation under maintained force that causes an increase in tissue rest length that may be considered a kind of permanent stretching (Blum et al., 2002). Some creep data have been published for human sclera and cornea (McBrien et al., 2009; Shchukin et al., 1998; Yoo et al., 2011b), chicken sclera (Lewis et al., 2014), and bovine extraocular muscles (Yoo et al., 2011a), and sclera (Myers et al., 2010b). However, creep of the optic nerve (ON) and its sheath have not been explored, to our knowledge. Characterization of creep for human posterior ocular tissues (Campbell et al., 2014) has become particularly important as it has recently become recognized that the ON constitutes a mechanical load on the eye during ductions that may contribute to development of myopia (Chang et al., 2017; McFadden and Wildsoet, 2020; Phillips et al., 2000) and optic neuropathy (Clark et al., 2020; Demer et al., 2017, 2020).

Whole eye inflation has been used for study of scleral creep because pressure can be uniformly applied to the entire intact eye (Lewis et al., 2014; Myers et al., 2010a; Myers et al., 2010b). However, this approach is unsuitable for the ON and its surrounding sheath. Acoustic methods have been developed to probe viscoelastic ocular tissue properties (Han et al., 2017; Ramier et al., 2019), but technical challenges for *in vivo* application to posterior ocular regions are substantial (Zvietcovich and Larin, 2022). Because of high attenuation, such high ultrasound intensity is necessary to image the posterior segment and orbit that human safety concerns limit available methods (Li et al., 2021). We therefore investigated ocular viscoelastic by uniaxial creep testing of fresh postmortem human tissues including sclera, ON, and the ON sheath.

Depending on material properties, the time and stress can be independent variables for a creep function (Provenzano et al., 2001). When creep is independent of stress level, the material is considered to exhibit linear viscoelasticity. A model consisting of springs and dashpots can describe viscoelastic properties of linear viscoelastic solids (De Pascalis et al., 2014), although individual elements of such a model need not have particular anatomical of physiological meaning. Nonlinear viscoelastic solids have been analyzed by formulations including Schapery's quasilinear viscoelasticity method (Schapery, 1969, 1992), and time-temperature-stress superposition (Luo et al., 2007a; Luo et al., 2007b). We hypothesized that sclera, ON, and ON sheath can be described by linear viscoelasticity, and if so, can be described by a lumped parameter model (Mattei and Ahluwalia, 2019) for compliance

of each tissue. We sought to determine if resulting empirical fits are reliable, and therefore useful to predict relaxation behavior.

2. Methods

2.1 Experimental Apparatus.

We constructed a tensile load cell with closed-loop control system to elongate tissues with a constant force inside a physiologically controlled chamber. The system consists of a linear motor (Ibex Engineering, Newbury Park, CA) having 100 mm/s maximum speed, a quadrature optical position encoder having 1 nm resolution, and a sensitive force sensor (LSB200, FUTEK, Irvine, CA) having 5 mN resolution. Via a frictionless air bearing, the linear motor shaft was coupled to a rod passing through a frictionless air bearing and attached at its distal end to a clamp for tightly gripping soft tissues within an environmental chamber maintaining approximately physiological temperature and humidity. Photographs of the apparatus have been published (Shin et al., 2018; Shin et al., 2015). The position, velocity, and acceleration of the actuator were independently controlled via custom software via digital serial communication to enable rapid application followed by closed-loop control of tension on the specimen. Measured force noise was reduced using a moving average filter with a 64 ms window. To maintain physiologic humidity and temperature, specimens were loaded in a nearly closed chamber in humid air above a heated water bath regulated to control air temperature near the specimen at 37C° measured by a thermocouple. Ringer's lactate solution (B. Braun Medical Inc., Bethlehem, PA, USA) warmed to bath temperature was continuously dripped onto the tissues to assure constant hydration. Dropwise liquid application did not produce detectable disturbance on the force sensor or linear motor.

2.2 Specimen Preparation.

Ten pairs of postmortem, Caucasian human eyes of average age 77 ± 17 years (5 male and 5 female) were harvested within 9 ± 5 hours of death by the Lions Gift of Sight Eye Bank (Saint Paul, MN, USA), air shipped on ice to the laboratory within 2 to 3 days postmortem, and processed as elsewhere described in detail (Park et al., 2021). Tissues were constantly moisturized with Ringer's lactate solution to prevent dehydration. Briefly, eyes were dissected into specimens of anterior, equatorial, posterior, and peripapillary sclera; ON; and ON sheath. Most tissues were shaped into rectangular specimens approximately 6 mm long by 2 mm wide with original thickness measured by a digital caliper (Mitutoyo Co., Kawasaki, Japan) so that cross sectional area was known for each specimen. For tensile loading, peripapillary sclera was oriented circumferentially to the optic disc. Since preliminary testing indicated that orientation of all other scleral specimens did not appreciably influence findings, equal numbers of specimens for each location were oriented radially and circumferentially. Specimens of ON and ON sheath were oriented to the long dimension of each tissue. In order to prevent slippage of ON and ON sheath specimens in the clamp, their ends were glued with cyanoacrylate to thin cardboard at each end.

2.3 Creep Testing.

Because human sclera is nearly isotropic (Eilaghi et al., 2010), we assumed isotopy and employed uniaxial loading. Preconditioning refers to initial cyclic loading to release stresses

resulting from specimen preparation and facilitate repeatable mechanical responses of biological tissues (Fung, 1973; Mainardi and Spada, 2011). Since we previously found that at least four loading cycles are required f or ocular tissues (Park et al., 2021), we preconditioned the tissues with 6 cycles at 5% strain. The force required to achieve 5% strain for the initial preconditioning cycle was recorded and served as target force for the remaining five preconditioning cycles and the entire creep trial. After preconditioning, the controller rapidly increased tension at strain rate 0.02 sec^{-1} until attaining 75% of target force, after which the rate of tension increase was reduced to avoid overshooting target force that was then maintained by negative feedback control at the target level. Target force was thus achieved within 2–3 sec after which it was maintained stable for 1,500 sec as force and displacement were sampled at 5 Hertz. This rate resulted in sampled 7,500 time points for each trial, and was sufficient to characterize relaxation times that all exceeded 5 sec.

2.4. Linearity of Viscoelasticity Theory.

To ascertain if linear viscoelasticity is appropriate, we compared the creep for the same regions under different stress levels. When tissues have linear viscoelasticity, creep patterns are independent of stress levels. If this is the case, then compliance *J(t)*, strain normalized by stress level, can be represented as a simple exponential function of time.

$$J(t) = \frac{\varepsilon}{\sigma} = at^n \tag{1}$$

where ε is strain, σ is applied stress, a is an arbitrary constant, t is time, and n is a curve fitting exponent. As a test for linear viscoelasticity, we determined exponent n as a function of stress magnitude by curve fitting for each specimen (Figure 1). The finding of a constant n value over the stress range would confirm linearity with respect to stress.

2.5. Time Dependence of Viscoelasticity.

The time dependence of a material within the linear viscoelastic range (Mattei and Ahluwalia, 2019) can be modeled as a combination of Maxwell and Kelvin-Voigt models (Ellard et al., 1986) (Byrne and Chaplain, 1996). Thus, the following expression described compliance *J(t):*

$$J(t) = a_1 t + a_2 - a_3 e^{-\frac{t}{a_4}} - a_5 e^{-\frac{t}{a_6}} - a_7 e^{-\frac{t}{a_8}} \tag{2}$$

where a_1, a_2, a_3, a_4, a_5, a_6, a_7, and a_8 are coefficients that are estimated by curve fitting. The curve fitting was performed by using the *fmincon* function in the MATLAB Optimization toolbox (MathWorks, Natick, MA, USA). No particular physical meaning is attributable to individual coefficients. Since Equation 2 does not assure that combinations of coefficients represent unique solutions, but only a sufficient description of compliance.

2.6. Sensitivity Analysis.

We performed a sensitivity analysis of compliance Equation 2 to variations in individual parameters. Average compliance was computed as its time integral divided by observation time. Sensitivity of average compliance to each individually varied parameter was computed as the rate of change of average compliance relative to that parameter.

2.7. Characteristic Time

Characteristic Time is defined by the temporal change in compliance, which is proportional to strain (Eqn. 1) since stress was held constant during testing. Therefore characteristic was conveniently determined from the time to for strain reach asymptote. By curve fitting, we obtained coefficients a_1 and a_2 for compliance in Equation 2 that reduces to a linear equation. We defined the characteristic time as the time when the difference between the linear equation and the measured compliance curve first declined to less than 5%.

2.8. Reduced Relaxation Function.

We estimated the reduced relaxation function from creep testing by using the Prony series (Loy et al., 2015). Curve fitting can approximate compliance in the form of $J(t) = a_1 t + a_2 - a_3 e^{-\frac{t}{a_4}} - a_5 e^{-\frac{t}{a_6}} - a_7 e^{-\frac{t}{a_8}}$. Relaxation modulus $G_R(t)$ is related to compliance as follows: $\int_0^t G_R(t-\tau)J(\tau)d\tau = t$. Since the relaxation modulus $G_R(t)$ can be represented in the form of $G_R(t) = g_1 e^{-t/\tau_1} + g_2 e^{-t/\tau_2} + g_3 e^{-t/\tau_3} + g_4 e^{-t/\tau_4}$, Substitution of the Prony series into the convolution equation gives the expanded equation.

$$\int_0^t \sum_{i=1}^{4} g_i e^{-\frac{t-\tau}{\tau_i}} \left(a_1\tau + a_2 - a_3 e^{-\frac{\tau}{a_4}} - a_5 e^{-\frac{\tau}{a_6}} - a_7 e^{-\frac{\tau}{a_8}} \right) d\tau = t \tag{3}$$

The equation can be converted into the form below, and integration by parts simplifies the equation.

$$\sum_{i=1}^{4} \int_0^t g_i e^{-\frac{t-\tau}{\tau_i}} \left(a_1\tau + a_2 - a_3 e^{-\frac{\tau}{a_4}} - a_5 e^{-\frac{\tau}{a_6}} - a_7 e^{-\frac{\tau}{a_8}} \right) d\tau = t \tag{4}$$

$$a_1 I_1(t,\ g_i,\ \tau_i) + a_2 I_2(t,\ g_i,\ \tau_i) - \sum_{i=1}^{3} a_{2i+1} \sum_{j=1}^{4} K_j = t \tag{5}$$

$$I_1 = \sum_{i=1}^{4} g_i \left(t\tau_i e^{\frac{t}{\tau_i}} + \tau_i^2 \left(e^{\frac{t}{\tau_i}} - 1 \right) \right) e^{-t/\tau_i}$$

(6)

$$I_2 = \sum_{i=1}^{4} g_i \tau_i e^{-\frac{t}{\tau_i}} \left(e^{\frac{t}{\tau_i}} - 1 \right)$$

(7)

$$K_j = \sum_{j=1}^{4} g_j e^{-\frac{t}{\tau_j}} \left(\frac{1}{\tau_j} - \frac{1}{a_{2i+2}} \right)^{-1} \left(e^{\left(\frac{1}{\tau_j} - \frac{1}{a_{2i+2}} \right)^{-1} t} - 1 \right)$$

(8)

The undetermined coefficients g_1, g_2, g_3, g_4, τ_1, τ_2, τ_3, and τ_4 were determined by the interior-point method (Mehrotra, 1992), which is a numerical scheme for nonlinear optimization. Then the time for $G_R(t)$ to decline to e^{-1} was taken to be the relaxation time. The ratio of the relaxation time to the observation time is the Deborah number (Huilgol, 1975; Reiner, 1964), a rheological term describing material fluidity relative to time scale of the process or behavior under consideration. The observation time for any Deborah number is not determined by the duration of the experiment performed, but by the interval relevant to the particular behavior. Therefore, in the current case the Deborah number depends on both the creep relaxation time, and the dynamics of the particular process or behavior under consideration. Observation times for relevant biological processes and behaviors are cited here from published data.

3. Results

3.1 Linearity.

To determine if tissues exhibit linear viscoelasticity, we performed linearity testing shown in Figure 1. Each point in the scatter plot represents the exponent describing creep for one specimen at stress level normalized to its maximum. We calculated Pearson's correlation coefficients for the relationship between these exponents and stress magnitudes. Correlation coefficients were 0.220, −0.229, 0.233, 0.146, 0.084, and 0.243, respectively, for the anterior, equatorial, posterior, peripapillary sclera, ON, and ON sheath. These correlation coefficients represent negligible correlations (Mukaka, 2012), so the tissues can be considered linearly viscoelastic.

3.2. Compliance Using Linear Viscoelasticity.

The data in Figure 2 illustrate that the ON is the most compliant of all tissues tested, whereas anterior sclera is the least compliant. The ON is much more compliant than its sheath. Equatorial sclera is the most compliant scleral region. Having verified linear viscoelasticity, we applied the lumped parameter model of Equation 2 to each tissue region (Figure 2), obtaining nonlinear coefficients of determination R^2 in every case of at least 0.998 that represents excellent fitting. Table 1 lists the fitted coefficients.

3.3. Sensitivity Analysis for Relaxation Coefficients.

To understand the significance of each coefficient in Equation 2, we calculated the relative changes of area under the compliance curve resulting from adjusting each coefficient individually. Increases by 20% in coefficients a_1, a_2, a_3, a_4, a_5, a_6, a_7, and a_8, areas under the curve changed by 6.2 ± 0.8%, 15.1 ± 1.7%, 0.33 ± 0.45%, 0.28 ± 0.37%, 0.25 ± 0.16%, 0.21 ± 0.13%, 0.76 ± 1.21%, and 0.60 ± 0.93% across all the specimens (Figure 3). Variations of coefficients a_1 and a_2 thus significantly affect areas under the compliance curve (Figure 3), whereas the remaining coefficients contribute little to variations in compliance.

The compliance curves therefore represent limiting behaviors after sufficient time, when behavior becomes dominantly linear and described by coefficients a_1 and a_2. We defined the creep characteristic time as the first time that the compliance curve approximates a linear approximation within 5%. The creep characteristic times for anterior, equatorial, posterior, peripapillary sclera, ON, and ON sheath are 193, 384, 341, 488, 984, and 256 sec, respectively. No characteristic time exceeded 1,500 sec. Because the compliance curves can be linearly approximated, we concluded that the observation time for these creep experiments was sufficient to describe the creep behaviors.

3.4. Derived Relaxation and Its Meaning.

Using the Prony series (Loy et al., 2015), we estimated reduced relaxation modulus (Sorvari and Malinen, 2006) for each region (Figure 4). We also defined the relaxation time for the relaxation modulus to decrease by a factor of e^{-1}, and the Deborah number that is the ratio of the stress relaxation time to the observation time or duration of an event (Huilgol, 1975; Reiner, 1964). The relaxation times for anterior, equatorial, posterior, peripapillary sclera, ON, and ON sheath are 73, 30, 35, 27, 5.6, and 25 sec, respectively. For heuristic purposes, we calculated example Deborah numbers for typical human pursuit tracking at 30°/s as an event lasting 1 sec; and for typical 10° and 40° saccades as events lasting 50 and 70 msec (Robinson, 2022), respectively. For these examples, we calculated illustrative Deborah numbers for anterior, equatorial, posterior, peripapillary sclera, ON, and ON sheath (Table 2). These numbers are not intended to be precise, but to indicate ranges or orders of magnitude to provide general insight about the importance of viscoelasticity during physiological eye movements. High Deborah numbers imply that the materials behave like solids, and conversely, low numbers imply fluid-like behavior. For pursuit tracking, all tissues exhibit Debora numbers less than 75, and should be regarded as viscoelastic. With a 5.6 Deborah number, the ON is particularly viscoelastic during slow eye movements such as pursuit and convergence, but viscoelasticity is also evident during these eye movements for ON sheath, and all scleral regions except for much anterior sclera.

4. Discussion

4.1. Context of Findings.

The visual system is inherently both sensory and motor. During fixation, an onging series of small saccades prevents perceptual fading and contribute to vision (Costela et al., 2013; McCamy et al., 2012). Larger saccades occur during wakefulness (Wu et al., 2013) and sleep (Leclair-Visonneau et al., 2010), and can be as large as 55° and as rapid as several

hundred degrees per second (Guitton and Volle, 1987). During free head and body motion, 25–45° saccades are observed (Anastasopoulos et al., 2009). With rare exceptions (David et al., 1997; Li et al., 2020; Suh et al., 2021), behavior of posterior ocular tissues has not been modeled during eye movements, largely because of the dearth of data on viscoelastic properties of these tissues. The present study demonstrates using creep testing that sclera, ON, and ON sheath have linear viscoelastic properties roughly independent of stress level. Not surprisingly, the ON is the most compliant tissue, and anterior sclera the least compliant. Compliance of posterior sclera and ON sheath are similar, as seemingly necessary to avoid marked mechanical discontinuities at their junction in the peripapillary region. Both of these tissues have much lower compliance than the highly compliant ON, presumably to provide strain relief to protect the soft ON from the forces generated by eye movements (East et al., 2019; Luchette et al., 2022).

4.2. Time Scaling of Ocular Compliance.

Compliance can be roughly judged by coefficient a_2 in Equation 2. By this measure, the ON is by far the most compliant, following by peripapillary sclera to which the ON joins at the optic disc. Compliances of the ON sheath, and posterior and equatorial sclera are less but closely matched, as would be expected to avoid stress discontinuities at their junction. Compliance is least for anterior sclera, as would be expected to support its role in stabilizing the optically critical cornea. Both ON and peripapillary sclera have relatively large coefficients a_1 and a_2 that represent fluid-like creep, as well as low Deborah numbers during even brief physiological eye movements that indicate tendency towards flow rather than rigidity. This is understandable for the ON with its soft neural tissue mixed with a sparser matrix of connective (Karim et al., 2004), and matching of the properties of its terminal junction with the eye to avoid stress concentration at material boundaries. However, since many eye movements end in sustained eccentric eye fixations or convergence for more than tens of seconds, viscoelastic effects become increasingly important at these longer time scales, even for stiffer scleral tissues. Compressive creep also exists (Yoo et al., 2011c), differing from tensile creep behavior (Yoon et al., 2000). Compressive creep studies of ocular tissues would also be worthwhile.

4.3 Comparison with Literature.

Prior studies have investigated ocular viscoelastic behavior. Downs et al. investigated stress relaxation in peripapillary sclera of normal rabbits and monkeys (Downs et al., 2003), monkeys with early experimental glaucoma (Downs et al., 2005), and pigs with and without glycosaminoglycan depletion (Hatami-Marbini and Pachenari, 2021), but did not perform creep testing. Downs *et al.* reported an instantaneous modulus of about 34 MPa for both normal and glaucomatous monkeys, but a greater equilibrium modulus of about 7.5 MPa in glaucomatous than 5 MPa in normal eyes (Downs et al., 2005). Elsheikh *et al.* (Elsheikh et al., 2010) and Karimi et al. (Karimi et al., 2017) noted evidence for viscoelastic behavior of human sclera when they reported an increase in tangent modulus with increasing tensile loading rate. Hatami-Marbini et al. reported scleral equilibrium modulus of 3–7 MPa in pigs (Hatami-Marbini and Pachenari, 2021). Ultrasound dynamic testing has been employed in canine sclera (Palko et al., 2011), but resulting storage and loss moduli are not directly

comparable to current creep data. Compressive stress relaxation data has been reported for mouse and pig sclera (Brown et al., 2021), and for pig optic nerve head (Safa et al., 2021).

4.4 Relevance to Modeling.

Although most previous studies have involved static and quasi-static phenomena (Jafari et al., 2021), the current data on creep properties of human posterior ocular tissues may also be useful for biomechanical modeling in relationship to axial myopia (McMonnies, 2014; Metlapally and Wildsoet, 2015; Ohno-Matsui and Jonas, 2019). Axial myopia represents eyeball elongation that stretches the retina and sclera as the eye enlarges. In progressive high myopia, the optic disc becomes progressively temporally tilted beginning in childhood (Samarawickrama et al., 2011); the adjacent retinal pigment epithelium progressively atrophies (Jonas, 2005; Lee et al., 1998; Savatovsky et al., 2015; Uchida et al., 1998) to progress into the macula where it often threatens central vision (Fang et al., 2018). Myopic macular degeneration may reduce visual acuity to blindness, in part through formation of local scleral ectasias called staphylomata (Li et al., 2019). Myopia, predominantly axial, has become epidemic (Verkicharla et al., 2016) in industrial societies, with prevalence ranging from 41% in the United States of America (Vitale et al., 2009) to 96% in Korea (Pan et al., 2015), and is increasing (Vitale et al., 2009) relentlessly as a public health crisis.

An association has been reported between creep characteristics of mammalian sclera and induced myopia (McBrien and Gentle, 2003; Phillips et al., 2000), including correlation between scleral elasticity and creep rate of human sclera (Dhakal et al., 2020; Jonas et al., 2020; McBrien et al., 2009). The high creep compliance of equatorial sclera may contribute to the formation of equatorial staphylomata in myopic eyes for which adjacent connective tissue ligaments of the orbital pulley system have degenerated and no longer provide external support to the equatorial sclera (Li et al., 2019). Such irregular staphylomata may in turn displace the paths of the extraocular muscles and contribute to strabismus (Demer, 2018).

4.5 Limitations.

While the current approach of testing human ocular tissues within three days of death probably represents a lower bound on the practical time scale of tissue freshness and is well within the range routinely employed for corneal transplantation into living recipients, it is possible that the values reported here may have been influenced by post-mortem changes. All specimens in the current study were from Caucasian donors, which should be considered since mechanical properties of sclera are known to vary according to race (Fazio et al., 2014). The current experiments were limited to tensile loading and could not address possible effects of anisotropy. However, it may be concluded that while on the rapid time scale of saccades the ON, ON sheath, and sclera behave as solids for which viscoelasticity may be neglected, for fixations and all other eye movements, viscoelastic behavior such as creep is important to understanding ocular biomechanics.

5. Conclusions

The human ON, its sheath, and the sclera exhibit creep consistent with linear viscoelasticity as evidenced by absence of correlation between creep rate and applied stress level. Thus, limiting creep behavior of these tissues may be characterized by lumped parameter compliance equations. The ON is the most compliant, and anterior sclera least compliant, with similar intermediate values for posterior sclera and ON sheath. These viscoelastic data may be understood through estimated Deborah numbers in context of well-established time scales for human eye movements. For pursuit tracking, all tissues exhibit Debora numbers less than 75, and should be regarded as viscoelastic. Because estimated Deborah number of the ON is less than 7 for pursuit and convergence, viscoelasticity is particularly important for these eye movements.

Financial Support:

USPHS National Institutes of Health grants EY008313 and EY00331, and an Unrestricted Grant to the Department of Ophthalmology from Research to Prevent Blindness. The funding organizations had no role in the design, conduct, or interpretation of this research.

References

Anastasopoulos D, Ziavra N, Hollands M, Bronstein A, 2009. Gaze displacement and inter-segmental coordination during large whole body voluntary rotations. Exp. Brain Res 193, 323–336. [PubMed: 19002676]

Blum W, Eisenlohr P, Breutinger F, 2002. Understanding creep - a review. Metallurgical and Materials Transactions a-Physical Metallurgy and Materials Science 33, 291–303.

Boote C, Sigal IA, Grytz R, Hua Y, Nguyen TD, Girard MJA, 2020. Scleral structure and biomechanics. Prog. Retin. Eye Res 74, 100773. [PubMed: 31412277]

Brown DM, Pardue MT, Ethier CR, 2021. A biphasic approach for characterizing tensile, compressive and hydraulic properties of the sclera. J R Soc Interface 18, 20200634. [PubMed: 33468024]

Byrne HM, Chaplain MAJ, 1996. The importance of constitutive equations in mechanochemical models of pattern formation. Applied Mathematics Letters 9, 85–90.

Campbell IC, Coudrillier B, Ross Ethier C, 2014. Biomechanics of the posterior eye: A critical role in health and disease. J. Biomech. Eng 136, 021005. [PubMed: 24356942]

Chang MY, Shin A, Park J, Nagiel A, Lalane RA, Schwartz SD, Demer JL, 2017. Deformation of optic nerve head and peripapillary tissues by horizontal duction. Am. J. Ophthalmol 174, 85–94. [PubMed: 27751810]

Clark RA, Suh SY, Caprioli J, Giaconi JA, Nouri-Mahdavi K, Law SK, Bonelli L, Coleman AL, Demer JL, 2020. Adduction-induced strain on the optic nerve in primary open angle glaucoma at normal intraocualr pressure. Curr. Eye Res 11, 1–11.

Costela FM, McCamy MB, Macknik SL, Otero-Millan J, Martinez-Conde S, 2013. Microsaccades restore the visibility of minute foveal targets. PeerJ 1, e119. [PubMed: 23940832]

David T, Smye S, James T, Dabbs T, 1997. Time-dependent stress and displacement of the eye wall tissue of the human eye. Med. Eng. Phys 19, 131–139. [PubMed: 9203147]

De Pascalis R, Abrahams ID, Parnell WJ, 2014. On nonlinear viscoelastic deformations: A reappraisal of fung's quasi-linear viscoelastic model. Proceedings of the Royal Society a-Mathematical Physical and Engineering Sciences 470.

Demer JL, 2018. Knobby eye syndrome. Strabismus 26, 33–41. [PubMed: 29279023]

Demer JL, Clark RA, Suh SY, Giaconi JA, Nouri-Mahdavi K, Law SK, Bonelli L, Coleman AL, Caprioli J, 2017. Magnetic resonance imaging of optic nerve traction during adduction in primary open-angle glaucoma with normal intraocular pressure. Invest. Ophthalmol. Vis. Sci 58, 4114–4125. [PubMed: 28829843]

Demer JL, Clark RA, Suh SY, Giaconi JA, Nouri-Mahdavi K, Law SK, Bonelli L, Coleman AL, Caprioli J, 2020. Optic nerve traction during adduction in open angle glaucoma with normal versus elevated intraocular pressure. Curr. Eye Res 45, 199–210. [PubMed: 31453714]

Dhakal R, Vupparaboina KK, Verkicharla PK, 2020. Anterior sclera undergoes thinning with increasing degree of myopia. Invest. Ophthalmol. Vis. Sci 61, 6.

Downs JC, Suh JK, Thomas KA, Bellezza AJ, Burgoyne CF, Hart RT, 2003. Viscoelastic characterization of peripapillary sclera: Material properties by quadrant in rabbit and monkey eyes. J. Biomech. Eng 125, 124–131. [PubMed: 12661206]

Downs JC, Suh JK, Thomas KA, Bellezza AJ, Hart RT, Burgoyne CF, 2005. Viscoelastic material properties of the peripapillary sclera in normal and early-glaucoma monkey eyes. Invest. Ophthalmol. Vis. Sci 46, 540–546. [PubMed: 15671280]

East L, Lyon M, Agrawal P, Islam Z, Newell M, Hockman T, Heger IM, Xu H, Kuchinski AM, Gibson RW, 2019. Increased intracranial pressure damages optic nerve structural support. J. Neurotrauma 36, 3132–3137. [PubMed: 31256706]

Eilaghi A, Flanagan JG, Tertinegg I, Simmons CA, Wayne Brodland G, Ross Ethier C, 2010. Biaxial mechanical testing of human sclera. J. Biomech 43, 1696–1701. [PubMed: 20399430]

Ellard CG, Goodale MA, Scorfield DM, Lawrence C, 1986. Visual cortical lesions abolish the use of motion parallax in the mongolian gerbil. Exp. Brain Res 64, 599–602. [PubMed: 3803494]

Elsheikh A, Geraghty B, Alhasso D, Knappett J, Campanelli M, Rama P, 2010. Regional variation in the biomechanical properties of the human sclera. Exp. Eye Res 90, 624–633. [PubMed: 20219460]

Fang Y, Yokoi T, Nagaoka N, Shinohara K, Onishi Y, Ishida T, Yoshida T, Xu X, Jonas JB, Ohno-Matsui K, 2018. Progression of myopic maculopathy during 18-year follow-up. Ophthalmology 125, 863–877. [PubMed: 29371011]

Fazio MA, Grytz R, Morris JS, Bruno L, Girkin CA, Downs JC, 2014. Human scleral structural stiffness increases more rapidly with age in donors of african descent compared to donors of european descent. Invest. Ophthalmol. Vis. Sci 55, 7189–7198. [PubMed: 25237162]

Fung YC, 1973. Biorheology of soft tissues. Biorheology 10, 139–155. [PubMed: 4728631]

Ghasia F, Wang J, 2022. Amblyopia and fixation eye movements. J. Neurol. Sci 441, 120373. [PubMed: 36007287]

Guitton D, Volle M, 1987. Gaze control in humans: Eye-head coordination during orienting movements to targets within and beyond the oculomotor range. J. Neurophysiol 58, 427–459. [PubMed: 3655876]

Han Z, Li J, Singh M, Wu C, Liu CH, Raghunathan R, Aglyamov SR, Vantipalli S, Twa MD, Larin KV, 2017. Optical coherence elastography assessment of corneal viscoelasticity with a modified rayleigh-lamb wave model. J. Mech. Behav. Biomed. Mater 66, 87–94. [PubMed: 27838594]

Hatami-Marbini H, Pachenari M, 2021. Tensile viscoelastic properties of the sclera after glycosaminoglycan depletion. Curr. Eye Res 46, 1299–1308. [PubMed: 34325593]

Huilgol R, 1975. On the concept of the deborah number. J Rheol (NY NY) 10, 297–306.

Jafari S, Lu Y, Park J, Demer JL, 2021. Finite element model of ocular adduction by active extraocular muscle contraction. Invest. Ophthalmol. Vis. Sci 62, 1.

Jonas JB, 2005. Clinical implications of peripapillary atrophy in glaucoma. Curr. Opin. Ophthalmol 16, 84–88. [PubMed: 15744137]

Jonas JB, Wang YX, Dong L, Guo Y, Panda-Jonas S, 2020. Advances in myopia research anatomical findings in highly myopic eyes. Eye Vis (Lond) 7, 45. [PubMed: 32905133]

Karim S, Clark RA, Poukens V, Demer JL, 2004. Quantitative magnetic resonance imaging and histology demonstrates systematic variation in human intraorbital optic nerve size. Invest. Ophthalmol. Vis. Sci 45, 1047–1051. [PubMed: 15037567]

Karimi A, Razaghi R, Navidbakhsh M, Ssera T, Kudo S, 2017. Mechanical properties of the human sclera under various strain rates: Elastic, hyperelastic, and viscoelastic models. J. Biomech. Tissue Eng 7, 686–695.

Kowler E, 2011. Eye movements: The past 25 years. Vision Res 51, 1457–1483. [PubMed: 21237189]

Leclair-Visonneau L, Oudiette D, Gaymard B, Leu-Semenescu S, Arnulf I, 2010. Do the eyes scan dream images during rapid eye movement sleep? Evidence from the rapid eye movement sleep behaviour disorder model. Brain 133, 1737–1746. [PubMed: 20478849]

Lee SB, Uhm KB, Hong C, 1998. Retinal vessel diameter in normal and primary open-angle glaucoma. Korean J. Ophthalmol 12, 51–59. [PubMed: 9753951]

Lewis JA, Garcia MB, Rani L, Wildsoet CF, 2014. Intact globe inflation testing of changes in scleral mechanics in myopia and recovery. Exp. Eye Res 127, 42–48. [PubMed: 25041940]

Li R, Du Z, Qian X, Li Y, Martinez-Camarillo JC, Jiang L, Humayun MS, Chen Z, Zhou Q, 2021. High resolution optical coherence elastography of retina under prosthetic electrode. Quant Imaging Med Surg 11, 918–927. [PubMed: 33654665]

Li Y, Singman E, McCulley T, Wu C, Daphalapurkar N, 2020. The biomechanics of indirect traumatic optic neuropathy using a computational head model with a biofidelic orbit. Front. Neurol 11, 346. [PubMed: 32411088]

Li Y, Wei Q, Le A, Gawargious BA, Demer JL, 2019. Rectus extraocular muscle paths and staphylomata in high myopia. Am. J. Ophthalmol 201, 37–45. [PubMed: 30731081]

Loy R, De Hoog F, Anderssen RS, 2015. Interconversion of prony series for relaxation and creep. J Rheol (NY, NY) 59, 1261–1270.

Luchette M, Helmke K, Maissan IM, Hansen HC, Stolker RJ, Tasker RC, Akhondi-Asl A, 2022. Optic nerve sheath viscoelastic properties: Re-examination of biomechanical behavior and clinical implications. Neurocrit. Care 37, 184–189. [PubMed: 35237919]

Luo WB, Wang CH, Zhao RG, Year Application of time-temperature-stress superposition principle to nonlinear creep of poly (methyl methacrylate). In Key Eng Mater.

Luo WB, Wang CH, Zhao RG, 2007b. Application of time-temperature-stress superposition principle to nonlinear creep of poly(methyl methacrylate). Engineering Plasticity and Its Applications from Nanoscale to Macroscale, Pts 1 and 2 340–341, 1091-+.

Mainardi F, Spada G, 2011. Creep, relaxation and viscosity properties for basic fractional models in rheology. European Physical Journal-Special Topics 193, 133–160.

Mattei G, Ahluwalia A, 2019. A new analytical method for estimating lumped parameter constants of linear viscoelastic models from strain rate tests. Mechanics of Time-Dependent Materials 23, 327–335.

McBrien NA, Gentle A, 2003. Role of the sclera in the development and pathological complications of myopia. Prog. Retin. Eye Res 22, 307–338. [PubMed: 12852489]

McBrien NA, Jobling AI, Gentle A, 2009. Biomechanics of the sclera in myopia: Extracellular and cellular factors. Optom. Vis. Sci 86, E23–30. [PubMed: 19104466]

McCamy MB, Otero-Millan J, Macknik SL, Yang Y, Troncoso XG, Baer SM, Crook SM, Martinez-Conde S, 2012. Microsaccadic efficacy and contribution to foveal and peripheral vision. J. Neurosci 32, 9194–9204. [PubMed: 22764228]

McFadden SA, Wildsoet C, 2020. The effect of optic nerve section on form deprivation myopia in the guinea pig. J. Comp. Neurol 528, 2874–2887. [PubMed: 32484917]

McMonnies CW, 2014. An examination of the baropathic nature of axial myopia. Clin. Exp. Optom 97, 116–124. [PubMed: 23937058]

Mehrotra S, 1992. On the implementation of a primal-dual interior point method. SIAM J Optim2, 575–601.

Metlapally R, Wildsoet CF, 2015. Scleral mechanisms underlying ocular growth and myopia. Prog. Mol. Biol. Transl. Sci 134, 241–248. [PubMed: 26310158]

Mukaka MM, 2012. Statistics corner: A guide to appropriate use of correlation coefficient in medical research. Malawi Med. J 24, 69–71. [PubMed: 23638278]

Myers KM, Cone FE, Quigley HA, Gelman S, Pease ME, Nguyen TD, 2010a. The in vitro inflation response of mouse sclera. Exp. Eye Res 91, 866–875. [PubMed: 20868685]

Myers KM, Coudrillier B, Boyce BL, Nguyen TD, 2010b. The inflation response of the posterior bovine sclera. Acta Biomater. 6, 4327–4335. [PubMed: 20558331]

Ohno-Matsui K, Jonas JB, 2019. Posterior staphyloma in pathologic myopia. Prog. Retin. Eye Res 70, 99–109. [PubMed: 30537538]

Palko JR, Pan X, Liu J, 2011. Dynamic testing of regional viscoelastic behavior of canine sclera. Exp. Eye Res 93, 825–832. [PubMed: 21983041]

Pan CW, Dirani M, Cheng CY, Wong TY, Saw SM, 2015. The age-specific prevalence of myopia in asia: A meta-analysis. Optom. Vis. Sci 92, 258–266. [PubMed: 25611765]

Park J, Shin A, Jafari S, Demer JL, 2021. Material properties and effect of preconditioning of human sclera, optic nerve, and optic nerve sheath. Biomech. Model. Mechanobiol

Phillips JR, Khalaj M, McBrien NA, 2000. Induced myopia associated with increased scleral creep in chick and tree shrew eyes. Invest. Ophthalmol. Vis. Sci 41, 2028–2034. [PubMed: 10892839]

Provenzano P, Lakes R, Keenan T, Vanderby R, 2001. Nonlinear ligament viscoelasticity. Ann. Biomed. Eng 29, 908–914. [PubMed: 11764321]

Ramier A, Tavakol B, Yun SH, 2019. Measuring mechanical wave speed, dispersion, and viscoelastic modulus of the cornea using optical coherence elastography. Opt. Express 27, 16635–16649. [PubMed: 31252887]

Reiner M, 1964. The deborah number. Physics Today 17, 62–62.

Robinson DA, 2022. Properties of rapid eye movements. Prog. Brain Res 267, 271–286. [PubMed: 35074058]

Safa BN, Read AT, Ethier CR, 2021. Assessment of the viscoelastic mechanical properties of the porcine optic nerve head using micromechanical testing and finite element modeling. Acta Biomater. 134, 379–387. [PubMed: 34274532]

Samarawickrama C, Mitchell P, Tong L, Gazzard G, Lim L, Wong TY, Saw SM, 2011. Myopia-related optic disc and retinal changes in adolescent children from singapore. Ophthalmology 118, 2050–2057. [PubMed: 21820741]

Savatovsky E, Mwanza JC, Budenz DL, Feuer WJ, Vandenbroucke R, Schiffman JC, Anderson DR, Ocular Hypertension Treatment S, 2015. Longitudinal changes in peripapillary atrophy in the ocular hypertension treatment study: A case-control assessment. Ophthalmology 122, 79–86. [PubMed: 25208858]

Schapery RA, 1969. On characterization of nonlinear viscoelastic materials. Polymer Engineering and Science 9, 295-+.

Schapery RA, 1992. On nonlinear viscoelastic constitutive-equations for composite-materials. Proceedings of the Vii International Congress on Experimental Mechanics, Vols 1 and 2, 9–21.

Shchukin ED, Izmailova VN, Larionova NI, Krasnov MM, Gurov AN, Bessonov AI, Afanas'eva GN, 1998. Creep of the eye sclera. Materials Research Innovations 2, 147–149.

Shin A, Park J, Demer JL, 2018. Opto-mechanical characterization of sclera by polarization sensitive optical coherence tomography. J. Biomech 72, 173–179. [PubMed: 29580690]

Shin A, Yoo L, Demer JL, 2015. Viscoelastic characterization of extraocular z-myotomy. Inv. Ophtalmol. Vis. Sci 56, 243–251.

Sorvari J, Malinen M, 2006. Determination of the relaxation modulus of a linearly viscoelastic material. Mech Time Depend Mater 10, 125–133.

Suh DW, Song HH, Mozafari H, Thoreson WB, 2021. Determining the tractional forces on vitreoretinal interface using a computer simulation model in abusive head trauma. Am. J. Ophthalmol 223, 396–404. [PubMed: 32663454]

Uchida N, Kiuchi Y, Miyamoto K, Uchida J, Tobe T, Tomita M, Shioda S, Nakai Y, Koide R, Oguchi K, 1998. Glutamate-stimulated proliferation of rat retinal pigment epithelial cells. Eur. J. Pharmacol 343, 265–273. [PubMed: 9570476]

Verkicharla PK, Chia NE, Saw SM, 2016. What public policies should be developed to cope with the myopia epidemic? Optom. Vis. Sci 93, 1055–1057. [PubMed: 27525536]

Vitale S, Sperduto RD, Ferris FL 3rd, 2009. Increased prevalence of myopia in the united states between 1971–1972 and 1999–2004. Arch. Ophthalmol 127, 1632–1639. [PubMed: 20008719]

Wu YM, Pietrone R, Cashmere JD, Begley A, Miewald JM, Germain A, Buysse DJ, 2013. Eeg power during waking and nrem sleep in primary insomnia. J. Clin. Sleep Med 9, 1031–1037. [PubMed: 24127147]

Yoo L, Kim H, Shin A, Gupta V, Demer JL, 2011a. Creep behavior of passive bovine extraocular muscle. J. Biomed. Biotechnol 2011, 526705. [PubMed: 22131809]

Yoo L, Reed J, Gimzewski JK, Demer JL, 2011b. Mechanical interferometry imaging for creep modeling of the cornea. Invest. Ophthalmol. Vis. Sci 52, 8420–8424. [PubMed: 21969299]

Yoo L, Reed J, Gimzewski JK, Demer JL, 2011c. Mechanical interferometry imaging for creep modeling of the cornea. Invest. Ophthalmol. Vis. Sci 52, 8420–8424. [PubMed: 21969299]

Yoon KJ, Wiederhorn SM, Luecke WE, 2000. Comparison of tensile and compressive creep behavior in silicon nitride. J. Am. Ceram. Soc 83, 217–222.

Zvietcovich F, Larin KV, 2022. Wave-based optical coherence elastography: The 10-year perspective. Prog Biomed Eng (Bristol) 4.

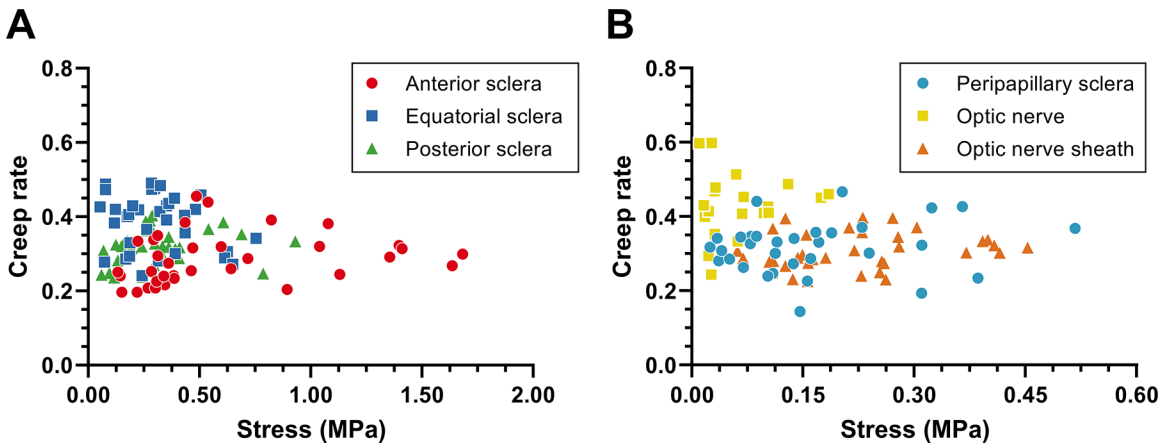

Figure 1.

Linearity test. Each symbol indicates one creep experiment for one specimen. Creep rate n is the exponent derived from a single term at^n (Equation 1). Linear viscoelasticity is appropriate because n values are independent of stress, and tissues from same region showed similar creep rate. Data for 32 samples of each scleral region and the optic nerve (ON) sheath, and 20 samples of ON.

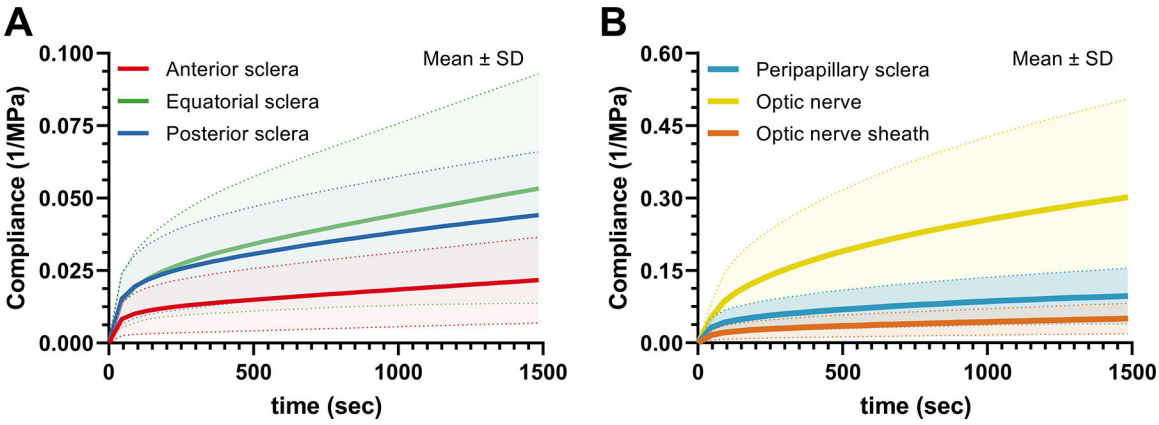

Figure 2.

Compliance curves. Creep is illustrated as compliance *J(t)* as a function of time (1,500 sec) in (A) various scleral regions, and (B) peripapillary sclera, ON, and its sheath. Regions with larger compliance are more viscoelastic.

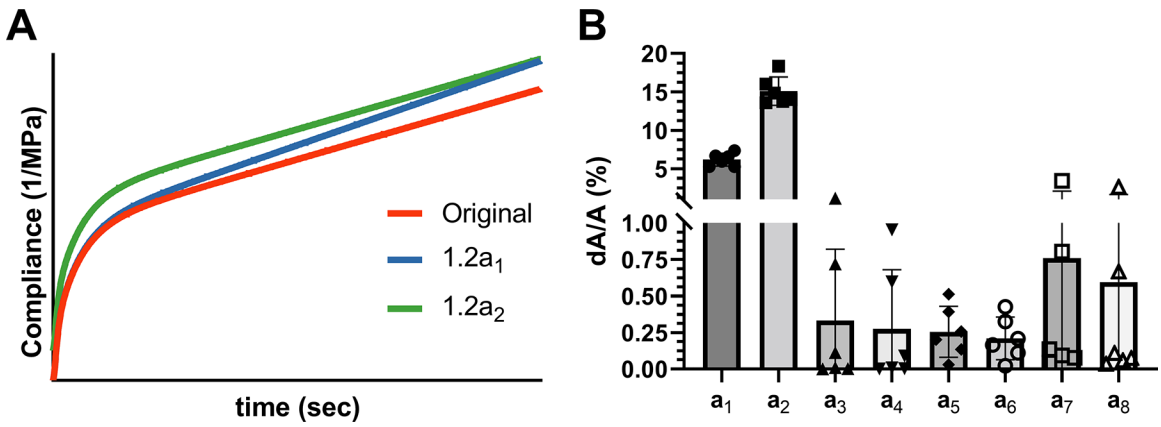

Figure 3.

Sensitivity analysis of Equation 2 for every specimen. (A) $1.2a_1$ and $1.2a_2$ indicate 1% increases of coefficients. The increased values changed the slopes and y-intercepts of the asymptotic line, and so are dominant factors. (B) Influences on relative changes of area under the compliance curve by 20% changes in individual coefficients.

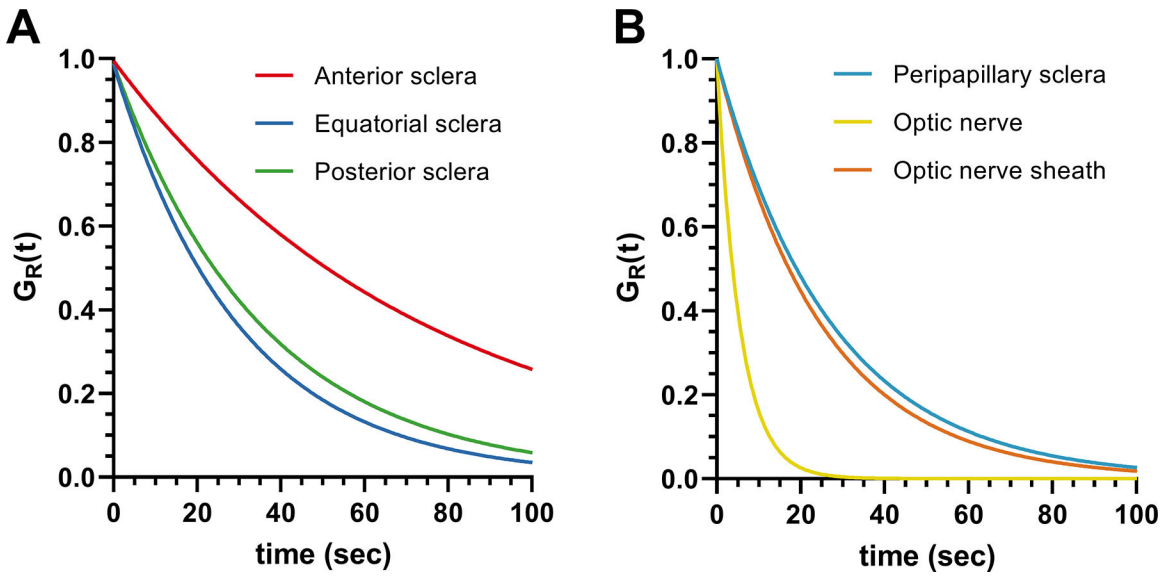

Figure 4.
Predicted reduced relaxation modulus

Table 1.

Coefficients for Relaxation Function (Equation 2)

	Anterior Sclera	Equatorial Sclera	Posterior Sclera	Peripapillary Sclera	Optic Nerve	Optic Nerve Sheath
a_1	7.5428×10^{-6}	1.8615×10^{-5}	1.3556×10^{-5}	2.7268×10^{-5}	7.6587×10^{-5}	1.7334×10^{-5}
a_2	0.01164	0.02574	0.02537	0.06249	0.20087	0.02771
a_3	0.00748	0.01229	0.01459	0.03233	0.13678	0.02032
a_4	66.1376	185.874	126.103	207.900	420.168	74.6826
a_5	0.00579	0.01497	0.02528	0.11165	0.08341	0.04514
a_6	9.13159	25.2781	9.08595	13.1199	39.0472	6.99692
a_7	−0.00163	−0.00152	−0.01449	−0.08149	−0.01932	−0.03776
a_8	2.16343	2. 24422	4.97760	9.37559	7.61441	5.60130

Table 2.

Deborah Numbers for Typical (Robinson, 2022) Smooth Pursuit and Saccades

	Anterior Sclera	Equatorial Sclera	Posterior Sclera	Peripapillary Sclera	Optic Nerve	Optic Nerve Sheath
Pursuit (30°/sec)	73	30	35	27	5.6	25
10° Saccade (200°/sec)	1480	600	705	548	113	503
40° Saccade (500°/sec)	1056	429	504	391	80	359